

PREPARATION OF SILVER-DOPED RICE HUSK SILICA COMPOSITES USING THE SOL-GEL METHOD

#PULUNG KARO-KARO*, SIMON SEMBIRING*, IQBAL FIRDAUS*, RUDY SITUMEANG**, SURIPTO DWI YUWONO**

*Department of Physics, Faculty of Mathematics and Natural Sciences, University of Lampung, Jl. Prof. Soemantri Brojonegoro, Bandar Lampung, 35145, Indonesia

**Department of Chemistry, Faculty of Mathematics and Natural Sciences, University of Lampung, Jl. Prof. Soemantri Brojonegoro, Bandar Lampung, 35145, Indonesia

#E-mail: pulung.karokaro@fmipa.unila.ac.id

Submitted April 25, 2022; accepted July 19, 2022

Keywords: Silica, Silver, Sol-gel, Ag-SiO₂ composites

Silver-doped rice husk silica composites were created using the sol-gel method. Silver nitrate and rice husks were used as the resources. The composites were sintered at 850 °C and then characterised using Fourier transform Infrared Spectroscopy (FTIR), X-ray diffractometry (XRD) coupled with a Rietveld analysis, Scanning Electron Microscopy-Energy Dispersive Spectroscopy (SEM/EDS), Ultraviolet-visible (UV-vis) spectroscopy and the Brunauer–Emmett–Teller (BET) method. The obtained results indicate the significant role of the Ag concentration and that the phase transformation changed the samples' characteristics, including an increased crystallite size and absorbance. The results also showed that the Ag/SiO₂ composite with a uniform microstructure in the form of spherical Ag particles with a relatively uniform size were dominated by silver and cristobalite phases as the main phases. Meanwhile, the silver phase emerged as a dominant phase and was embedded in the silica matrix. The crystal sizes of the silver and cristobalite were found to be 40 and 20 nm, respectively. The absorbance value showed that Ag/SiO₂ works on two wavelengths of 310 and 415 nm. The obtained surface area values ranged from 5.0 - 11.4 m²·g⁻¹ which belongs to the mesopore criteria. Such structural and textural properties of the produced composite indicate its suitability to be used as a catalyst.

INTRODUCTION

Silver has gained greater attention in material technologies due to its great potential, such as its ability to be used as a catalyst [1, 2], in optoelectronics [3], chemical and biological sensing [4], as well as having antibacterial and antifungal properties [5, 6]. Silver particles are capable of reducing microbial growth even at very low concentrations. Silver can also be used as a protective coating and as innovative multifunctional composite. For example, silver particles have the potential for advanced optoelectronic devices and sensors [7]. Silver also has high electrical and thermal conductivity, at $6.3 \times 10^7 \text{ S}\cdot\text{m}^{-1}$ and $429 \text{ W}\cdot\text{m}^{-1}\cdot\text{K}^{-1}$ [8-9], which are practically useful for metal nanowire materials [10]. Therefore, it easily mixes with different inorganic materials, such as SiO₂, TiO₂, ZnO, SiO₂-TiO₂ [11-14] and results in new characteristics. Several researchers have inserted silver particles into a silica matrix of various forms, such as rods [15], powders [16], and monoliths [17] for antibacterial applications. Mohd, et al. 2019 [18] found that spherical silver particles on the silica surface with a particle size of 10 - 40 nm have a potential to be a catalyst in dye treatments.

Other than silver, SiO₂ has been used as a substrate to immobilise precious metals such as TiO₂ [19], Au [20], and Ni [21]. Bare metal particles are active and have a higher tendency to combine in the solution state due to van der Waals bonds compared to the solid state. Silica is biocompatible, porous, and highly reactive. Therefore, it can form chemical bonds with metal substrates and can bind directly to various ions and organic molecules in pores and surfaces. It has been known for decades that rice husks can be a source of silica via thermal and alkaline processes. With the thermal method, rice husk produces husk ash which is dominated by silica and can be used as an economic raw material. With the alkaline method [22-25], silica of high purity, activity, and an amorphous level can be obtained as a sol for easy use in synthesising materials using the sol-gel method. In several studies, silica from rice husks has been successfully used as a production material for silica-bitumen composites [26-28], a nanosilica [29-31], and a ferrisilicate [32].

Its characteristics allow the silica to be used as a convenient carrier agent to help mitigate the accumulation of silver particles and to accelerate their dispersion to produce Ag/SiO₂ composites at the desired performance. Several researchers have synthesised

Ag/SiO₂ composites, and obtained Ag/SiO₂ composite structures with particle sizes of 20 - 40 nm at a sintering temperature of 800 °C [33]. Sintering at 1000 °C also results in a stable structure without silver loss due to evaporation [34]. However, most silver experiences evaporation loss at a sintering temperature of 1060 °C and such evaporation is not detectable at a sintering temperature above 1110 °C. Nonetheless, cristobalite and tridymite crystals are formed at 1060 °C and 1080 °C, respectively. Furthermore, research conducted [35] with a silver concentration of 0.02 - 0.06 M after sintering at 500 °C showed that the phase formed was dominated by silica with no silver present. However, silver was detected with an increasing silver concentration above 0.06 M. This indicates that silver particles were trapped in the silica matrix. This composite was found to exhibit optical limiting properties. This finding also explains the interaction between the electrostatic repulsion of silica spheres and silver particles that form the structural arrangement of the synthesised silver-silica composite.

This work presents a collection of data obtained for sol-gel-derived solution from various silver concentrations to form Ag/SiO₂ composites. The composites have been developed for antibacterial and environmental applications. The main focus of this study is to determine the optimal silver concentration additions, which allow the formation of the Ag/SiO₂ composite structure. Therefore, it is essential to characterise the structural changes in details by adding silver to the silica matrix to obtain the Ag/SiO₂ composites. For this purpose, infrared (IR) spectroscopy, X-ray diffraction (XRD), SEM/EDS, UV-vis spectroscopy and the BET method were employed to determine the characteristic correlations from various silver concentrations.

EXPERIMENTAL

Materials

The raw rice husk was obtained from a local rice milling industry. Before use, the husk was soaked in hot water and left overnight. The floating husks were discharged, while the sinking husks were collected, rinsed with distilled water, and then oven dried at 110 °C for eight hours. A 5 % sodium hydroxide solution, a 10 % nitrate acid solution, and silver nitrate (98 % purity), ethanol and deionised/distilled water were used where reagent grade materials were purchased from Merck (KGaA, Darmstadt, Germany).

Preparation of the silica and silver sols

The rice husk silica was extracted using an alkali extraction process, as used in previous research [26]. Fifty grams (50 g) of the dry husk was put into a beaker glass containing 500 mL of 5 % NaOH. The mixture was boiled for 30 minutes and left to cool down to room

temperature and further left for 24 hours to optimise the release of the silica from the husk. The mixture was filtered to separate the dissolved silica (silica sol), with the rest being discharged. Afterwards, in order to obtain the silver solution at various concentrations (0.3, 0.4, 0.5, 0.6, 0.7 and 0.8 M), an amount of AgNO₃ powder was placed into 100 mL of distilled water and stirred using a magnetic stirrer for 30 minutes at a temperature of 110 °C. This resulted in a yellowish silver solution ready to be used as the silver sol.

Synthesis of the Silver-Silica (Ag/SiO₂) composites

To obtain a solid Ag/SiO₂ composite, silica and silver sols with the same volume of 100 mL were placed in separate beakers. First, the silver sol at different concentrations (0.3, 0.4, 0.5, 0.6, 0.7 and 0.8 M) was poured into the silica sol, and a 10 % HNO₃ solution was dripped in while stirring continuously. The complete procedure can be seen in a previous article [36]. The composite was then ready for analysis.

Characterisation

The effects of various silver concentrations on the structural evolution of the silica matrix were studied using spectroscopic measurements. Analysis of the functional groups was performed using a Perkin Elmer FTIR spectrometer in the range of 4000 - 500 cm⁻¹ in a diffuse reflectance mode using potassium bromide (KBr)-based pellets. The crystalline phase of the powder was characterised using XRD patterns with Cu K_α radiation ($\lambda = 0.154$ nm). Refinements were performed using the Rietica program version 1.70 for Windows 95/98/NT [37]. The microstructure of the thermally polished and etched samples was analysed using a Philips-XL SEM. The UV/Vis spectra of the samples were recorded from 250 to 800 nm. The Brunauer–Emmett–Teller (BET) surface area of the samples was then studied using a surface area analyser (Quantachrome Novawin-version 11.0).

RESULTS AND DISCUSSION

Functional group characteristics of the Ag/SiO₂ composites

Figure 1 shows the IR-spectra of the various Ag concentrations in the composites sintered at 850 °C. For all the samples, the strong bands are located at 1050 and 788 cm⁻¹ and are associated with the silica network. These are assumed to be the asymmetric and symmetrical vibrations of the Si-O-Si and O-Si-O functional groups in the SiO₄ tetrahedral, respectively, as reported by other researchers [38-40]. However, particular attention should be noted by the appearance of the peaks at 1050 cm⁻¹ and

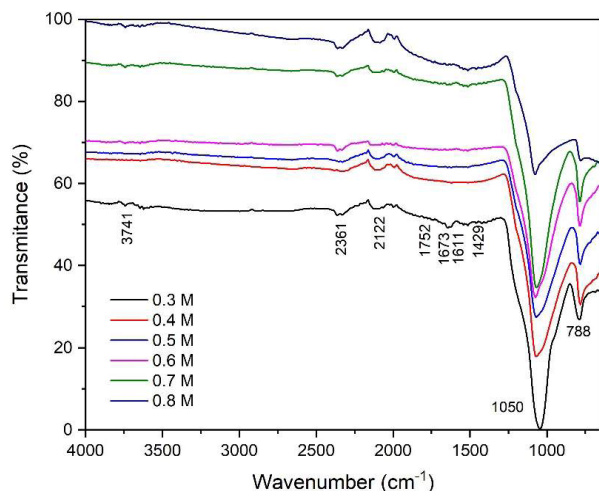


Figure 1. The FTIR spectra of the various Ag concentrations in the composites sintered at 850 °C.

788 cm^{-1} that are narrower. This behaviour is related to the formation of the Ag-O-Si bond [41], proving that the crystallisation of Ag-silica occurred in this composite. This observation is identical to the results derived from its diffractogram.

The small peak located at 3741 cm^{-1} for almost all the various Ag concentration in the composite (Figure 1) is usually associated with the O-H bond stretching vibration and the hydrogen bonds forming the silanol groups. This is also supported by the presence of a low band at 1673 cm^{-1} due to the H-O-H deformation that interacts via the hydrogen bonding with the silanol group [42]. All the samples also showed that the O-H groups disappear due to the thermal processes in this study. This phenomenon indicates the elimination of the hydroxyl groups in the solid powders. The re-emergence of the asymmetrical Si-O-Si stretching mode seems to indicate the Ag binding to the oxygen of the siloxane bond which occurs as the water molecules evacuate and the siloxane bond is re-established. Small peaks appearing at 1611 and 1752 cm^{-1} mark the vibrational strain of the C=C group and C=O bond of carboxylic acid as reported in earlier studies [43-45]. Another small peak observed at 2361 and 2122 cm^{-1} may be attributed to the presence of the O-H functional groups which is characteristic of carboxylic acids and C-H which is characteristic of alkanes. A gradual decrease in the NO_3^- ions with an increase in the Ag concentration in the composite could be due to the strong pyrolysis of AgNO_3 when sintered at 850 °C, releasing Ag atoms and NO_2 gas.

Structural characteristics of the Ag-SiO₂ composites

Figure 2 shows the XRD results of the various Ag concentrations in the Ag-SiO₂ composites. Phases formed were observed with a PDF diffraction line [46], with the main phases being cristobalite 21.9° (PDF-39-1425) and Ag 38.9° (PDF-4-0862).

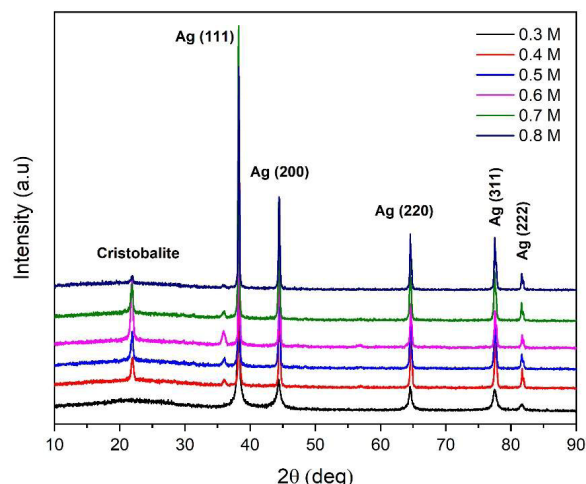


Figure 2. XRD patterns of the various Ag concentrations in the Ag/SiO₂ composites using CuK_α radiation sintered at 850 °C.

Figure 2 shows that for the XRD spectrum of the Ag-SiO₂ composite at 0.3 M Ag, a peak at $2\theta = 22^\circ$ is attributed to the amorphous silica matrix. This amorphous silica structure is due to the agglomeration of silver covering the formation of silica crystalline on the surface, as also observed by other researchers [47]. In addition to the obtained amorphous silica, strong peaks at $2\theta = 38.9^\circ, 48.5^\circ, 63.0^\circ, 77.5^\circ$ and 82.6° correlate to the (111), (200), (220), (311) planes and (222) orientations, which can be matched according to face-centre cubic (fcc) structure of Ag. This silver existence confirms that the Ag particles distributed on the cristobalite surface formed an fcc pattern of Ag-SiO₂ composites, which also agrees with the results from previous studies [48-52]. In other words, the presence of silver and silica phases indicates that, under these conditions, the formation of an Ag/SiO₂ composite starts with the deposition of Ag particles on the silica surface. An increase in the Molar Ag is found to be different from that of the 0.3 M Ag sample. When the sample was at 0.4 M Ag (Figure 2), it was associated with an increase in the structural order of the amorphous silica phase towards the cristobalite crystalline phase, compared to the observed sample at 0.3 M (Figure 2). Under these conditions, conversion of amorphous silica to cristobalite takes place. The presence of cristobalite is due to the crystallisation of the rice husk silica during thermal treatment, as is evident in previous research [53]. Interestingly, these changes may be related to the FTIR changes (see Figure 1), as both these changes are caused by an increase in the order of atomic arrangement.

The 0.4 to 0.8 M (Figure 2) samples concentrations were characterised by the clearly detectable presence of cristobalite and silver phases. The decrease or increase in both phases is attributed to the reaction to form Ag/SiO₂ composites via interdiffusion of cristobalite and silver atoms. Another difference with the various silver concentrations is the crystallisation variability of the silica

matrix, as the silver amount increases. Figure 2 shows that the intensity of the cristobalite and silver increases with an increase in the Ag concentration in the range of 0.4 to 0.6 M, while the cristobalite intensity decreases and the silver intensity increases at an Ag concentration at 0.7 and 0.8 M, respectively. The relative intensities at the silver peak (111) were higher than those of other peaks at each concentration. This indicates the preferential plane orientation to the silica surface. The increasing silver concentration results in more intense and narrower silver crystal diffraction peaks. This means that the average size of the silver particles increases. The crystallite size is estimated by analysing the broadening of the (111) and (101) reflections for silver and cristobalite, respectively. The crystallite size can be calculated using the Scherer formula [54].

Figure 3 shows the crystallite size of the various Ag concentrations in the Ag/SiO₂ composites. The crystallite size value of the crystalline silver is larger than that of the silica, which indicates that the agglomerates of silver particles formed during sintering temperature of 850 °C are embedded in the silica matrix. The crystallite size of the cristobalite and silver increases rapidly at an Ag concentration of 0.4 M. This is followed by a gradual decrease for the Ag concentrations from 0.4 to 0.6 M Ag

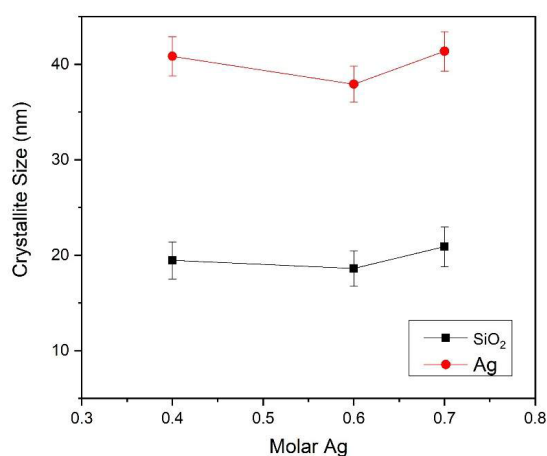


Figure 3. Crystallite size of the various Ag concentrations in the Ag/SiO₂ composites sintered at 850 °C.

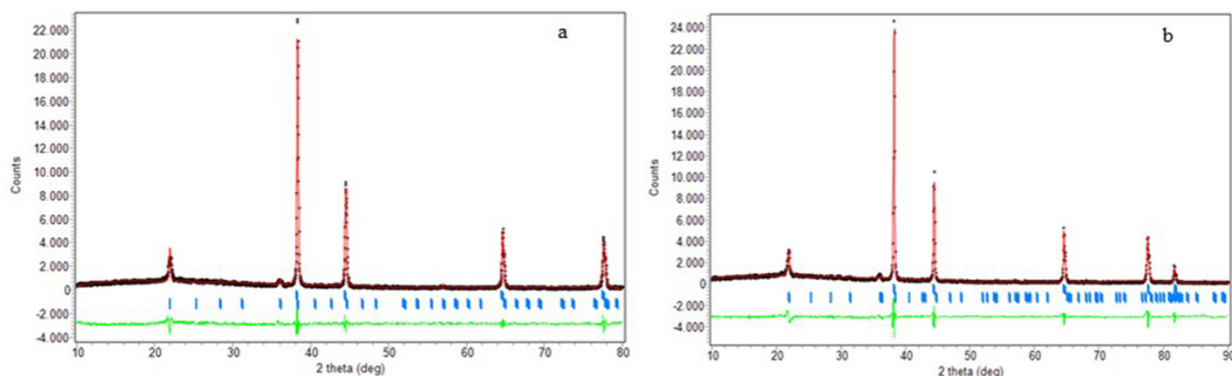


Figure 4. XRD Rietveld plot for the samples with various concentrations of Ag using CuK_α Radiation; (a) 0.4 M; (b) 0.7 M.

and another gradual increase at an Ag concentration of 0.7 M. This phenomenon indicates that the increase in the concentration from 0.4 M Ag to 0.7 M Ag does not significantly affect the particle size, but it does affect the silver dispersion that enters the silica matrix. For this reason, Ag particles are diffused into the silica particles, and, hence, increases the crystallite size of silver. This result strengthens the previous work [36].

In order to verify the XRD results, a Rietveld analysis was used to obtain quantitative information on the phase composition of the samples. The refined XRD patterns of the samples at Ag concentrations of 0.4 M and 0.7 M are shown in Figure 4. Table 1 presents the structure of the best fits and quantitative results calculated by the Rietveld method for all the samples. The R_{wp} , R_{exp} , R_p and goodness of fit (GoF) parameters indicate the quality of fitting values which is, in this case, relatively low according to the basic principle of GoF [55]. Therefore, perfect agreements were observed between the measured and calculated patterns. Table 1 shows that the amount of silica decreases slowly as the Ag concentration increases. This means that Ag is dispersed in the silica matrix. These results are supported by the presence of the Si, O and Ag elements using EDX that indicates formation of the Ag/SiO₂ composites, even without the presence of the other elements. The silica quantity slowly decreases while the silver quantity slowly increases as the Ag concentration increases.

Table 1. Figure-of merits (FOMS) and weight percentage (wt. %) of Ag and SiO₂ from the XRD data refinements for the samples with the different Ag concentrations.

Concentration of AgNO ₃ (M)	R_{wp}	R_p	R_{exp}	GoF	SiO ₂ (wt. %)	Ag (wt. %)
0.3	7.04	6.78	3.87	3.30	72.98	27.02
0.4	10.40	5.50	3.21	3.57	72.15	27.85
0.5	7.21	6.09	4.25	2.87	71.85	28.15
0.6	9.65	5.91	5.50	3.07	71.08	28.92
0.7	7.67	8.06	4.41	3.02	70.40	29.60
0.8	10.40	5.97	6.40	2.72	69.74	30.26

Microstructure characteristic of the Ag/SiO₂ composites

Figure 5a-c shows the surface morphologies of the Ag/SiO₂ composites with the different Ag concentrations. Meanwhile, Table 2 presents the significant presence of silver and silica with differences in the grain boundary size and particle distribution on the surface. The surface morphologies of the samples are marked by particles with different grain sizes and distributions. The microstructure of the sample with a 0.3 M Ag concentration (Figure 5a) reveals almost the same characteristic as that of the sample treated at 0.4 M Ag (Figure 5b). The samples prepared at 0.3 and 0.4 M (Figure 5a-b) concentrations are marked by large grains with less evident spherical particles, compared to those observed for other sample (Figure 5c). In addition, the clusters in the samples prepared at 0.3 and 0.4 M concentrations are surrounded by both medium sized and fine grains of silver, respectively. However, in the clusters prepared by other Ag concentrations, the crystalline of cristobalite still exists in the Ag/SiO₂ composites, surrounded by both medium sized and fine grains of silver.

Table 2. Chemical composition of the various Ag concentrations in the Ag/SiO₂ composites.

Sample (Ag Molar)	O (wt. %)	Si (wt. %)	Ag (wt. %)	Na (wt. %)
0.3*	52.25	27.23	20.52	-
0.4	43.86	23.66	32.48	-
0.5*	41.08	21.12	37.80	-
0.6	42.58	18.36	38.19	0.87
0.7	44.05	16.15	38.61	1.18
0.8*	44.05	15.15	39.61	1.18

Note: *) data is taken from the previous work [36]

The sample surfaces prepared at higher Ag concentrations (0.4 and 0.6 M) are dominated by larger grains composed of cristobalite clusters and are covered by some spherical particles of silver. Both samples are marked by initiated spherical particles of silver on the silica surface. This feature suggests that at the 0.4 and 0.6 M Ag concentrations, the cristobalite and silver phases continue to contact and allow those particles to interact, and, hence, form Ag/SiO₂ composites. This evolution is supported by the results of the XRD analysis for the samples at 0.3 M through 0.7 M, as shown in Figure 2, in which a silica amorph was detected. Formation of Ag/SiO₂ composites can be clearly observed through the SEM micrograph examination of the treated sample at a 0.7 M concentration (Figure 5c), which shows intensive spherical particles across its surface as Ag the concentration increases. This agglomeration results in increased interactions between the silver and silica and is followed by the intensive formation of Ag-SiO₂, as re-

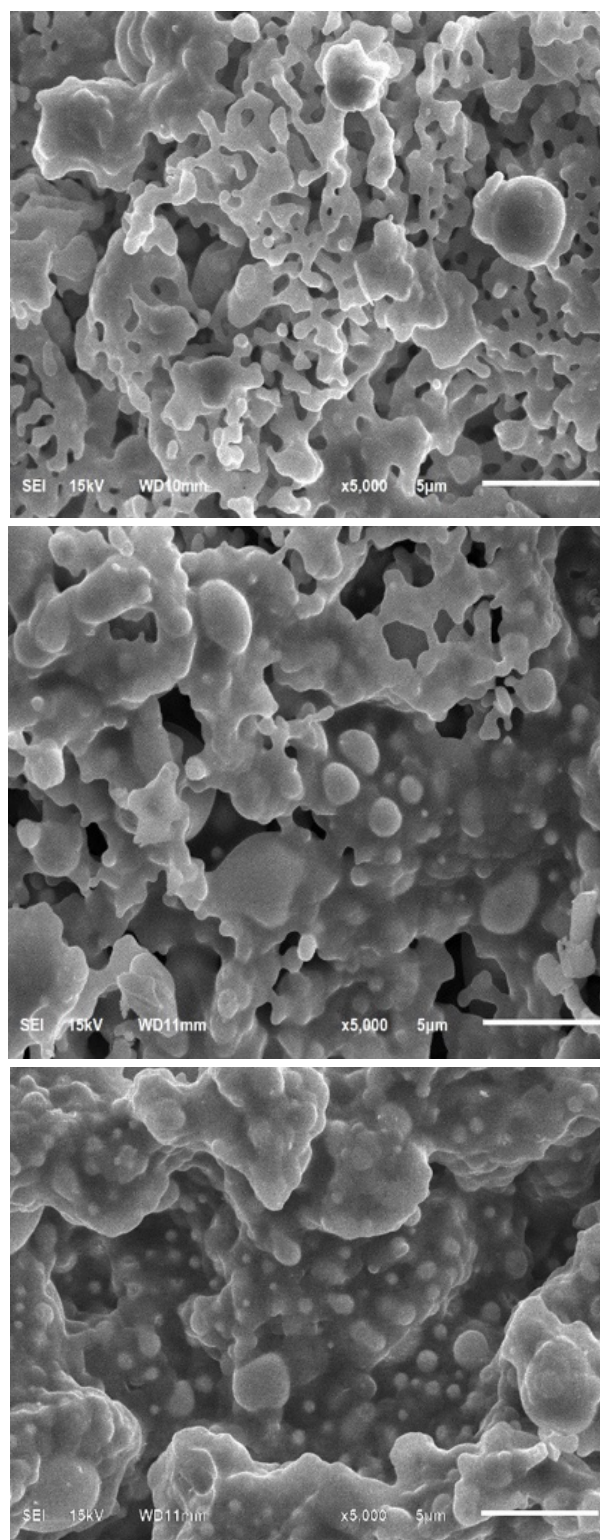


Figure 5. Morphologies of the various Ag concentrations in the Ag/SiO₂ composites sintered at 850 °C, magnification 5 kX, (a) 0.4 M, (b) 0.6 M, and (c) 0.7 M

vealed from the XRD observations. This phenomenon confirms that at concentration range of 0.4 - 0.7 M, the cristobalite phase reacts with the silver phase to form an Ag-SiO₂ composite. Moreover, the microstructure of the samples was found to display spherical particles

with relatively uniform sizes on the silica surface. These surface characteristics suggest that, at these concentrations, silver particles undergo a diffusion process that evenly spreads into the cristobalite particles, and, hence, encourages an increase in Ag/SiO₂ as the dominant phase, as verified by the XRD results.

The EDX data presented in Table 2 show the significant effect of the various Ag concentrations in the Ag/SiO₂ composites. The results from the elemental composition analysis indicate the significant effect of the different silver concentrations. At an Ag concentration of 0.4 M, the silica contains a significant amount of silver (23.66 wt. %), which decreases to 16.15 wt. % at an Ag concentration up to 0.7 M. Meanwhile, at an Ag concentration of 0.4 M, the silica contains a significant amount of Ag (32.48 wt. %), which increases to 38.61 wt. % at an Ag concentration of 0.7 M. The sample surfaces containing Ag concentrations of 0.4, 0.6, and 0.7 M (Figure 5a-c) are marked by fine grains of silver structure that cover several large grains of the cristobalite structure. The XRD results (Figure 2) reveal that these are composed of cristobalite and silver. Due to the agglomeration, the silver group interacts with the cristobalite, and, hence, the size of the cristobalite phase becomes smaller. The presence of silver and cristobalite phases in the last four composite samples suggests that the cristobalite phase continues to interact and allows the particles re-arrangement, leading to the formation of an Ag/SiO₂ composite. The interesting results from all the samples, both from the structural and microstructural characteristics, show that the Ag ions from the silver nitrate change to Ag particles, and, hence, form an Ag phase. This is proven by both the XRD and UV-vis results. In addition, the results of the microstructural analysis using SEM for all the samples indicate that the Ag particles are well dispersed in the silica matrix and that most of the particles are almost spherical in shape.

Optical characteristics of the Ag/SiO₂ composites

The data obtained from the SEM/EDX and XRD data were complemented with the observations of the Ag/SiO₂ composite formation using UV-visible spectroscopy. Figure 6 shows the optical absorbance spectra of the various Ag concentrations in the Ag/SiO₂ composites.

Figure 6 shows two intense broad bands and small band peaked at around 310, 415 and 450 nm, respectively, that are caused by the silver in contact with the silica particles. The absorbance peak of around 310 and 415 nm indicates the presence of Ag particles to form Ag/SiO₂ composites, as was also found by previous researchers [56]. These results show that silver phases dominate the sample surfaces with a silver absorption spectrum peak ranging from 350 to 390 nm [57].

The 415 nm absorbance peak is caused by surface plasmon excitation; a phenomenon that exists at the interface between a metal and a dielectric material [58]. The third peak (450 nm) is caused by aggregates of silver particles; a well-known phenomenon also found in other metals. For silver, such a reflection band was recently described by Martinez-Castanon, et.al., 2005 [59]. They also found that silver peaks at around 500 nm. Based on Figure 6, all the samples have two working regions of wavelengths at 310 nm and 415 nm. As for the changes in the Ag concentration, the sample with a concentration of 0.8 M Ag has the maximum absorption at the 310 nm wavelength. In comparison, the sample with the 0.5 M Ag concentration has a maximum absorption at the 410 nm wavelength.

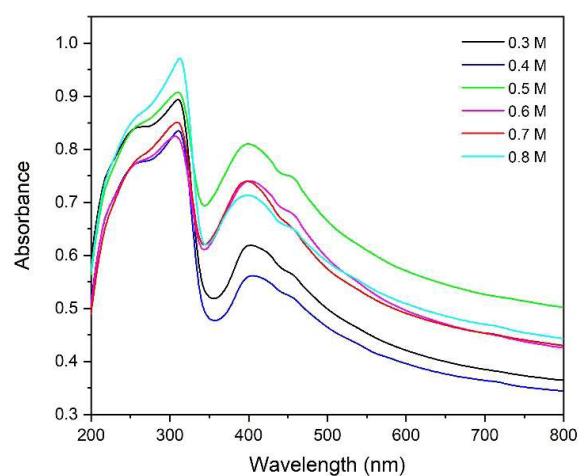


Figure 6. Absorption spectra of the various Ag concentrations in the Ag/SiO₂ composites sintered at 850 °C.

Surface area (BET) characteristics of the Ag/SiO₂ composites

Figure 7 shows the representative nitrogen adsorption-desorption isotherms for all the Ag/SiO₂ composites at various Ag concentrations. Meanwhile, the porous characteristics of the Ag/SiO₂ composites are given in Table 3. The graph shows that conspicuous hysteresis loops at a relative pressure are observed. These results indicate the typical characteristics of mesopores with a narrow pore size distribution. The phenomena are usually related to the capillary agglomeration associated with large pore channels, as also found in previous research [60]. Such a loop may exhibit a wide variety of shapes. This is also attributed to the presence of aggregates of plate-like particles that gave rise to slit-shaped pores. Table 3 shows that pore size distributions of the various Ag concentrations, from 0.3 up to 0.5 M Ag, in the Ag/SiO₂ composites have a wider pore size distribution than those with concentrations from 0.6 up to 0.8 M. This indicates the influence of silver on the

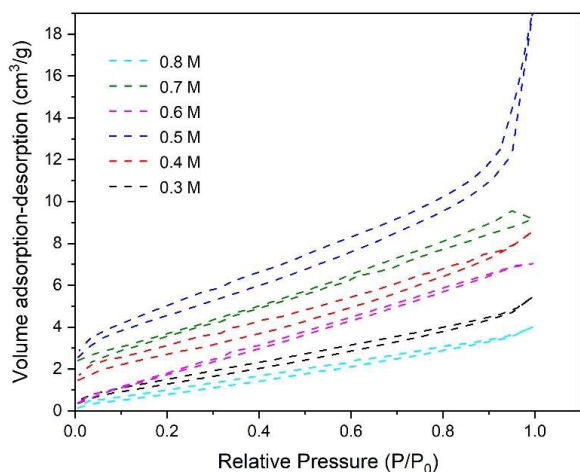


Figure 7. Nitrogen adsorption-desorption isotherms and of the various Ag concentrations in the Ag/SiO₂ composites sintered at 850 °C

Table 3. The porous of the various Ag concentrations in Ag/SiO₂ composites.

Sample (Ag Molar)	BET (surface area) (m ² ·g ⁻¹)	Total pore volume (m ³ ·g ⁻¹)	Average pore size (nm)	Particle size (μm)
0.3	5.732	0.007969	2.78069	2.5
0.4	7.318	0.001106	3.02155	1.5
0.5	11.400	0.002624	4.60270	0.5
0.6	10.109	0.001031	2.06953	0.6
0.7	9.961	0.000114	2.25565	1.5
0.8	5.052	0.006001	2.37562	2.0

properties of the Ag/SiO₂ composites. This, in turn, implies that surface area increases for Ag concentrations of 0.3 M to 0.5 M, and conversely, surface area decreases for Ag concentrations from 0.6 M to 0.8 M, as given in Table 3.

Figure 8 shows the pore distribution of the Ag/SiO₂ composites. The samples are mostly mesopores with a size smaller than 3 nm and estimated pore size probability from peak position is about 1.2 nm with a relatively narrow pore size distribution. Figure 8 also

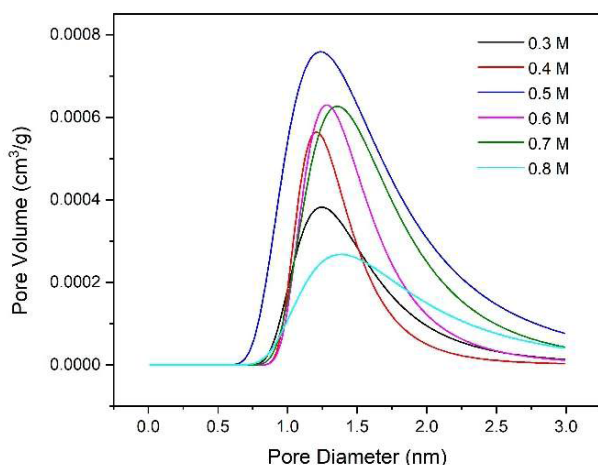


Figure 8. Pore distribution of the various Ag concentrations in the Ag/SiO₂ composites sintered at 850 °C.

shows that the pore distribution for all the samples is uniform. The shift in the pore distribution to small pores is due to the presence of some silver particles within the silica host matrix or the dispersion of the Ag particles inside the porous silica.

CONCLUSION

This study successfully demonstrated the preparation of Ag/SiO₂ composites using the sol-gel process by mixing rice husk silica and silver nitrate as the raw materials. The XRD data revealed the formation of Ag/SiO₂ composites, in which, at an Ag concentration of 0.3 M to 0.7 M, it results in major phases of silver and cristobalite. The silver phase emerged as the dominant phase that is embedded in the silica matrix. The phase transformation was found to cause changes in the sample characteristics related to the formation of silver, including an increased crystallite size and absorbance. The UV-vis absorption spectra revealed that Ag/SiO₂ works on two absorption bands at 310 nm and 415 nm wavelengths. Silver and cristobalite crystals were found to be 40 and 20 nm in size, respectively. From all the samples, the obtained surface area values ranged from 5.0 to 11.4 m²·g⁻¹, with the largest one obtained at a 0.5 M Ag concentration and it belongs to the mesopores criteria. The characteristics of the structure, microstructure, absorption bands, and mesopores found in this study suggest that the observed samples have the potential to be used as catalysts.

REFERENCES

- Chimentão R.J., Kirm I., Medina F., Rodríguez X., Cesteros Y., Salagre P., Sueiras J.E., Fierro L.G. (2005): Sensitivity of styrene oxidation reaction to the catalyst structure of silver nanoparticles. *Applied Surface Science*, 252, 793-800. doi:10.1016/j.apsusc.2005.02.064
- Long S., Li L., Guo H., Yang W., Lu F. (2012): Preparation of stable core-shell dye adsorbent Ag-coated silica nanospheres as a highly active surfaced-enhanced Raman scattering substrate for detection of rhodamine 6G. *Dyes and Pigments*, 95(3), 473-477. Doi:10.1016/j.dyepig.2012.05.023
- Guo L., Guan A., Lin X., Zhang C., Chen G. (2010): Preparation of a new core-shell Ag/SiO₂ nanocomposite and its application for fluorescence enhancement. *Talanta*, 82, 1696-1700. doi:10.1016/j.talanta.2010.07.051
- Baheiraei N., Moztafzadeh F., Hedayati M. (2012): Preparation and antibacterial activity of Ag/SiO₂ thin film on glazed ceramic tiles by sol-gel method. *Ceramics International*, 38, 2921-2925. doi: 10.1016/j.ceramint.2011.11.068
- Chaloupka K., Malam Y., Seifalian A.M. (2010): Nanosilver as a new generation of nanoparticle in biomedical applications. *Trends Biotechnology*, 28 (11), 580-588. Doi: 10.1016/j.tibtech.2010.07.006

6. Sotiriou G.A., Pratsinis S.E. (2010): Antibacterial activity of nanosilver ions and particles. *Environmental Science Technology*, 44 (14), 5649-5654. doi:10.1021/es101072s
7. David D., Evanoff Jr., Chumanov G. (2005): Synthesis and optical properties of silver nanoparticles and arrays. *Chem-PhysChem*, 6 (7); 1221-1231. doi:10.1002/cphc.200500113
8. Fahad S., Yu H., Wang L., Nazir A., Ullah R.S., Naveed K.U.R., Elshaarani T., Amin B.U., Khan A., Mehmood S. (2019): Synthesis of silver nanowires with controlled diameter and their conductive thin films. *Journal of Materials Science: Materials in Electronics*, 30, 12876-12887. Doi: 10.1007/s10854-019-01649-7
9. Mi H.Y., Li Z., Turng, L.S., Sun Y., Gong S., (2014): Silver nanowire/thermoplastic polyurethane elastomer nanocomposites: Thermal, mechanical, and dielectric properties. *Materials and Design*, 56, 398-404. Doi: 10.1016/j.matdes.2013.11.029
10. Lee J.H., Lee P., Lee D., Lee S.S., Ko S.H. (2012): Large-scale synthesis and characterization of very long silver nanowires via successive multistep growth. *Crystal Growth & Design*, 12(11) 5598-5605. doi:10.1021/cg301119d
11. Amornpitoksuk P., Suwanboon S., Sangkanu S., Sukhoom A., Muensit N., Baltrusaitis J. (2012): Synthesis, characterization, photocatalytic and antibacterial activities of Ag-doped ZnO powders modified with a diblock copolymer. *Powder Technology*, 219, 158-164. Doi: 10.1016/j.powtec.2011.12.032
12. Sun B., Sun S., Li T., Zhang W. (2007): Preparation and antibacterial activities of Ag-doped SiO₂-TiO₂ composite films by liquid phase deposition (LPD) method. *Journal of Material Science*, 42(24), 10085-10089. doi:10.1007/s10853-007-2109-5
13. Sobana N., Muruganadham M., Swaminathan M. (2006): Nano-Ag particles doped TiO₂ for efficient photodegradation of direct azo dyes. *Journal of molecular catalysis a chemical*, 258, 124-132. doi:10.1016/J.MOLCATA.2006.05.013.
14. Kawashita M., Tsuneyama S., Miyaji F., Kokubo T., Kozuka H., Yamamoto K. (2000): Antibacterial silver-containing silica glass prepared by sol-gel method. *Biomaterials*, 21, 393-398. doi:10.1016/s0142-9612(99)00201-x
15. Chahadih A., El Hamzaoui H., Cristini O., Bigot L., Bernard R., Kinowski C., Bouzaoui M., Capoen B. (2012): H₂-induced copper and silver nanoparticle precipitation inside sol-gel silica optical fiber preforms. *Nanoscale Research Letters*, 7, 487. Doi:10.1186/1556-276X-7-487
16. Hilonga A., Kim J.K., Sarawade P.B., Quang D.V., Shao G., Elineema G.H.T., Kim H.T. (2012): Silver-doped silica powder with antibacterial properties. *Powder Technology*, 215-216, 219-222. doi:10.1016/j.powtec.2011.09.051
17. Duhana S.N., Kishoreb P., Aghamkarc, Devi S., (2010): Preparation and characterization of sol-gel derived silver-silica nanocomposite. *Journal of Alloys and Compounds*, 57, 101-104. Doi: 10.1016/j.jallcom.2010.07.107
18. Ram D.C. (2012): Microstructure and surface morphology of nanocrystalline silver silicates. *Acta Physica Polonica A*, 121, 2000-2002.
19. Mohd N.K., Afiq W.M., Khalik A.A. Azmi A.A. (2019): Synthesis and characterization of silica-silver core-shell nanoparticles. *Malaysian Journal of Analytical Sciences*, 23(2), 290-299. doi:10.17576/mjas-2019-2302-13
20. Kitsou I., Panagopoulos P., Maggos T., Arkas M., Tsetsekou A. (2018): Development of SiO₂-TiO₂ core-shell nanospheres for catalytic applications. *Applied Surface Science*, 441, 223-231. doi:10.1016/j.apsusc.2018.02.008
21. Kandpal D., Kalele S., Kulkarni S.K. (2007): Synthesis and characterization of silica-gold core-shell (SiO₂-Au) nanoparticles. *Pramana*, 69(2), 277-283. doi:10.1007/s12043-007-0128-z
22. Alvarez J., Lopez G., Amutio M, Bilbao J., Olazar M., (2014): Upgrading the rice husk char obtained by flash pyrolysis for the production of amorphous silica and high-quality activated carbons. *Biosource Technology*, 170, 132-137. doi:10.1016/j.biortech.2014.07.073
23. Gu S., Zhou J., Luo Z. (2015): Kinetic study on the preparation of silica from rice husk under various pretreatments. *Thermal Analysis Calorimetry*, 119, 2159-2169. doi:10.1007/s10973-014-4219-z
24. Sankar S., Sharma S.K., Kaur N., Lee B., Kim D.Y., Lee S., Jung H. (2016): Biogenerated silica nanoparticles synthesized from sticky, red, and brown rice husk ashes by chemical method. *Ceramic International*, 42, 4875-4885. Doi: 10.1016/j.ceramint.2015.11.172
25. Feng Q., Chen K.D., Ma D. (2018): Synthesis of high specific surface area silica aerogel from rice husk ash via ambient pressure drying. *Colloid and Surface*, 539(1205), 399-406. doi: 10.1016/j.colsurfa.2017.12.025
26. Sembiring S., Riyanto A., Situmeang R., Sembiring Z. (2019): Bituminous Composite Comprising Amorphous Silica from Rice Husks. *Ceramics-Silikáty*, 63(3), 277-286. doi: 10.13168/cs.2019.0021
27. Sembiring S., Riyanto A., Situmeang R., Sembiring Z., Susanti N., Firdaus I. (2020): Effect of amorphous rice husk silica addition on the structure of asphalt composite. *Metals Materials and Minerals*, 30(4), 113-118. doi: 10.14456/jmmm.2020.59
28. Sembiring S., Agus riyanto A., Firdaus I., Junaidi, Ningtias E.A., Situmeang R. (2021): Structural characterisation of asphalt-rice husk silica composites. *Ceramics-Silikáty*, 65(3), 215-223. doi: 10.13168/cs.2021.0021
29. Sarangi M., Bhattacharyya S., Behera R.C. (2009): Effect of temperature on morphology and phase transformations of Nano crystalline silica obtained from rice husk. *Phase Transitions*, 282(5), 377-386. doi:10.1080/01411590902978502
30. Soltani N., Bahrami A., Pech-Canul M.I., Gonzales L.A. (2015): Review on the physiochemical treatments of rice husk for production of advanced materials. *Chemical Engineering*, 264, 899-935. doi:10.1016/j.cej.2014.11.056
31. Bathla A., Narulal C., Chauhan R.P. (2018): Hydrothermal synthesis and characterization of silica nanowires using rice husk ash: an agricultural waste. *Material Science Material in Electronic*, 29(8), 6225-6231. Doi: 10.1007/s10854-018-8598-y
32. Bhagiyalakshmi M., Auradha R., Palanichamy M., Jang H.T. (2010): Dexterous template-free synthesis of ferrisilicate with MFI morphology using rice husk ash. *Journal of Non Crystalline Solids*, 356(23-24), 1204-1209. doi:10.1016/j.jnoncrysol.2010.04.017
33. Pham D.P., Huynh K.K., Tran C.V., Vu V.Q., Tran T.T.V. (2014): Preparation and structural characterization of sol-gel-derived silver silica nanocomposite powders. *International Journal of Materials Science and Applications*, 3(5), 147-151.
34. Dudek K., Podwórny J., Dulski M., Nowak A., Peszke J. (2017): X-ray investigations into silica/

- silver nanocomposite. *Powder Diffraction*, 32(S1), 1-5. doi:10.1017/S0885715617000185
35. Anand P.B., Suchand Sandeep C.S., Kishore Sridharan, Narayanan T.N., Thomas S., Philip R., Anantharaman M.R. (2012): An Optical Limiter Based on Silver-Silica. *Advanced Science, Engineering and Medicine*, 4, 33-38. doi:10.1166/asem.2012.1115
36. Sembiring S., Riyanto A., Firdaus I., Junaidi., Situmeang R. (2022): Structure and Properties of Silver-Silica Composite prepared from Rice husk Silica and Silver Nitrate. *Ceramics-Silikaty* 66, 167-177. doi: 10.13168/cs.2022.0011
37. Hunter B.A. (1997). *Software Rietica for 95/98 Window NT*. Version 1.70.
38. Racles C., Nistor A., Cazacu M.A. (2013): silica-silver nanocomposite obtained by sol-gel method in the presence of silver nanoparticles. *Central European Journal of Chemistry*, 1(10), 1689-1698. doi: 10.2478/s11532-013-0294-4
39. Duhan S., Devi S., Srivastava M. (2010): Characterisation of nanocrystalline Ag/SiO₂ nanocomposite and synthesis by wet chemical method. *Indian Journal of Pure and Applied Physics*, 48, 271-275.
40. Music S., Filipovic-Vincekovic N., Sekovanic L. (2011): Precipitation of amorphous SiO₂ particles and their properties. *Brazilian Journal. of Chemical. Engineering*, 28, 89-94. doi:10.1590/S0104-66322011000100011
41. Abbass A.B., Van Vuuren A.J., Swart H.C., Kroon R.E., (2017): Distinguishing the nature of silver incorporated in sol-gel silica. *Journal of Non-Crystalline Solids*, 475, 71-75. doi:10.1016/j.jnoncrysol.2017.08.033
42. Mitra J., Ghosh M., Bordia R.K., Sharma A. (2013): Photoluminescent electrospun submicron fibers of hybrid organosiloxane and derived silica. *RSC Advances*, 3, 7591-7600. Doi: 10.1039/C3RA23408H
43. Bruni S., Cariati F., Casu M., Lai A., Musinu A., Piccaluga G., Solinas S. (1999): IR and NMR study of nanoparticle-support interactions in Fe₂O₃-SiO₂ nanocomposite prepared by a sol-gel method. *Nanostructure Material*, 11, 573-586. doi: 10.1016/S0965-9773(99)00335-9
44. Ahsani M., Sabouri R., Ulbricht M., Hazrati H., Jafarizad A., Yegani R. (2021): Preparation and characterization of hydrophilic and antibacterial silver decorated silica-grafted-poly (vinylpyrrolidone) (Ag-SiO₂-PVP) nanoparticles for polymeric nanocomposites. *Journal of Applied Polymer Science*, e50977, 1-12. doi: 10.1002/app.50977
45. Javadi M., Jafarzadeh Y., Yegani R., Kazemi S. (2018): PVDF membranes embedded with PVP Functionalized nanodiamond for pharmaceutical wastewater treatment. *Chemical Engineering Research Design*, 140, 241-250. doi:10.1016/j.cherd.2018.10.029
46. Powder Diffraction File (Type PDF-2), (1997). *Diffraction Data for XRD Identification*. International Centre for Diffraction Data, PA, USA.
47. Prakash P., Gnanaprakasam P., Emmanuel R., Arokiyaraj S., Saravanan M. (2010): Green synthesis of silver nanoparticles from leaf extract of *Mimusops elengi*, Linn. for enhanced antibacterial activity against multi drug resistant clinical isolates. *Colloids and Surfaces B: Biointerfaces*, 108, 255-259. doi:10.1016/j.colsurfb.2013.03.017
48. Shalaka A.M., Pratik R.C., Vrishali B.S., Suresh P.K. (2011): Rapid biosynthesis of silver nanoparticles using *Cymbopogon citratus* (Lemongrass) and its antimicrobial Activity. *NanoMicro Letters*, 3, 189-194. doi:10.1007/BF03353671
49. Din L.B., Mie R., Samsudin M.W., Ahmad A., Ibrahim N. (2015): Biomimetic synthesis of silver nanoparticles using the lichen *Ramalina dumeticola* and the antibacterial activity. *Malaysian Journal of Analytical Sciences*, 19 (2), 369-376.
50. Chen K.H., Pu Y.C., Chang K.D., Liang Y.F., Liu C.M., Yeh J.W., Shih H.C., Hsu Y.J. (2012): Ag-nanoparticle-decorated SiO₂ nanospheres exhibiting remarkable plasmon-mediated photocatalytic properties. *The Journal of Physical Chemistry C*, 116 (35), 19039-19045. doi:10.1021/jp306555j
51. Kordatos K., Gavela S., Ntziouni A., Pistiolas K.N., Kyritsi A., Kasselouri V. (2008): Synthesis of highly siliceous ZSM-5 zeolite using silica from rice husk ash. *Microporous and Mesoporous Materials*, 115, 189-196. doi:10.1016/j.micromeso.2007.12.032
52. Yao D.D., Murata H, Tsunega S., and Jin R.H. (2015): Chiral SiO₂ and Ag/SiO₂ Materials Templated by Complexes Consisting of Comblike Polyethyleneimine and Tartaric Acid. *Chemistry European Journal*, 21, 15667-15675. doi: 10.1002/chem.201502290
53. Zhuravlev L.T. (2000): The surface chemistry of amorphous silica. Zhuravlev model. *Colloid Surface A. Physicochemical and Engineering Aspects*, 173, (1-3); 1-38. doi:10.1016/S0927-7757(00)00556-2
54. Cullity B.D. (1978). *Elements of X-Ray Diffraction*. 2nd ed. Department of Metallurgical Engineering and Materials Science University of Notre Dame. Addison-Wesley Publishing Company Inc.
55. Kisi E.H. (1994): Rietveld analysis of powder diffraction patterns. *Material Forum*, 18, 135-153.
56. Lungulescu E.M., Sbarcea G., Setnescu R., Nicula N., Ducu R., Lupu (Luchian) A.M., Ion I., Marinescu V. (2019): Gamma Radiation Synthesis of Colloidal Silver Nanoparticles. *Revista de Chimie*, 70 (8), 2826-2850.
57. Yan Y., Chen K., Li H., Hong W., Hu X., Xu Z. (2014): Capping Effect of Reducing Agents and Surfactants in Synthesizing Silver Nanoplates. *Transactions of Nonferrous Metals Society of China*, 24 (11), 3732-3738. doi:10.1016/S1003-6326(14)63522-6
58. Jeon H.J., Yi S.C., Oh S.G. (2003): Preparation and antibacterial effects of Ag SiO₂ thin films by sol-gel method. *Biomaterials*, 24, 4921-4928. doi: 10.1016/S01429612(03)00415-0
59. Martinez-Castanon G., Martinez J.R., Zarzosa O.G., and Ruiz F., (2005): Optical Absorption of Ag Particles Dispersed in a SiO₂ Amorphous Matrix. *Journal of sol-gel science and technology*, 36(2), 137-145. Doi: 10.1007/s10971-005-5285-2
60. Sing K.S.W., Everett D.H., Haul R.A.W., Moscou L., Pierotti R.A., Rouquerol J., Siemieniowska L. (1985): Reporting Physisorption Data for Gas/Solid Systems with Special Reference to the Determination of Surface Area and Porosity. *Pure and Applied Chemistry*. 57 (4), 603-619. Doi: 10.1351/pac198557040603